# The Rubredoxin from *Clostridium pasteurianum*: Mutation of the Conserved Glycine Residues 10 and 43 to Alanine and Valine

**Mustafa Ayhan,[†] Zhiguang Xiao,[†] Megan J. Lavery,[†] Amanda M. Hamer,[†] Kerry W. Nugent,[†] Sergio D. B. Scrofani,[†] Mitchell Guss,[‡] and Anthony G. Wedd*[,†]**

Schools of Chemistry and Physics, University of Melbourne, Parkville, Victoria 3052, Australia, and Department of Biochemistry, University of Sydney, Sydney, NSW 2006, Australia

*Received December 28, 1995*[⊗]

Conserved glycine residues at positions 10 and 43 in the electron transfer protein rubredoxin (active site: Fe(Cys-*S*)$_4$) from *Clostridium pasteurianum* are related by a pseudo-2-fold symmetry. They have been mutated to alanine and valine and four single and two double mutant (G10V/G43A and G10V/G43V) proteins expressed in stable form in *Escherichia coli.* Physical properties were modified by steric interactions between the $\beta$- and $\gamma$-carbon substituents of the new side chains and the CO functions of C9 and C42 and other adjacent groups. These interactions perturb the chelate loops formed by residues 5−11 and 38−44. $^1$H NMR results for Cd(II) forms indicate that the Pr$^i$ side chain of V10 in the G10V mutant occupies the surface pocket defined by loop 5−11 and thereby modifies the environment of the 5−11 NH protons. The equivalent side chain of V43 in G43V is denied the same access to the 38−44 pocket. This leads to a specific perturbation of the V44−NH···S−C42 interaction in this mutant. These effects are additive in the double mutant G10V/G43V, consistent with the different structural changes being localized in each loop. The midpoint potentials of the iron forms of the six mutants are shifted negatively relative to the recombinant protein by −16 to −86 mV. A G → V mutation has a larger effect than a G → A, but again, an additivity of the differential effects is seen in the double mutants. Minor perturbations of resonance Raman and electronic spectra are dominated by the mutation at G10. Overall, the present work represents one approach to the systematic exploration of the influence of the protein chain upon the fundamental properties of this molecule.

## Introduction

The simplest of the iron−sulfur proteins are the rubredoxins (Rd) which feature a single Fe(Cys-*S*)$_4$ site in a protein of molar mass approximately 6000 Da.[1−5] They are presumed to be electron transport proteins, and this role has been demonstrated in both the sulfate-reducing bacterium *Desulfovibrio gigas* and the aerobe *Pseudomonas aleovorans.*[6,7] The protein from the latter organism is more complex, with two iron sites in a molar mass of 15 000 Da. In *Desulfovibrio* bacteria, there are a number of proteins which contain at least two iron atoms.[8−11] In addition to Rd-like sites,[10] some of these contain other iron centers which feature fewer than four cysteinyl ligands.[8,9]

The rubredoxin from the dinitrogen-fixing bacterium *Clostridium pasteurianum*, Rd*Cp*, has been examined in some detail.[1,2,5] It has now been expressed in *Escherichia coli*,[12,13] providing ample recombinant protein rRd*Cp* for further study.[14] Generation of mutant forms has begun.[15,16]

Thirteen Rds have been sequenced, and all conserve the four Cys ligands (amino acid residues 6, 9, 39, and 42 in Rd*Cp*) and the three residues (Gly-10, Pro-40, Gly-43) involved in the formation of the tight turns of the "chelate loops" defined by residues 5−11 and 38−44 (Chart 1a).[4,12] In each of the centers defined by X-ray crystallography,[4] the Fe(Cys-*S*)$_4$ site and the peptide backbone atoms of the loops exhibit a pseudo-2-fold symmetry which includes six NH···S interactions (Figure 1). Using the type I−IV classification for such hydrogen bonds,[17] the sulfur atoms of buried metal ligands Cys-6 and Cys-39 each interact with two peptide NH functions (types I and III), while surface metal ligands Cys-9 and Cys-42 interact with one only (type II) (Chart 1b; Figure 1b).

* To whom correspondence should be addressed at the School of Chemistry, University of Melbourne, E-mail: T.Wedd@chemistry.unimelb.edu.au.
[†] University of Melbourne.
[‡] University of Sydney.
[⊗] Abstract published in *Advance ACS Abstracts,* August 15, 1996.

(1) Eaton, W. A.; Lovenberg, W. *Iron-Sulfur Proteins*; Academic Press: New York, 1973; Vol. II, pp 131.
(2) Watenpaugh, K. D.; Sieker, L. C.; Jensen, L. H. *J. Mol. Biol.* **1979**, *131*, 509. (b) *J. Mol. Biol.* **1980**, *138*, 615.
(3) Day, M. W.; Hsu, B. T.; Joshua-Tor, L.; Park, J.-B.; Zhou, Z. H.; Adams, M. W. W.; Rees, D. C. *Protein Sci.* **1992**, *1*, 1494.
(4) Sieker, L. C.; Stenkamp, R. E.; LeGall, J. *Methods Enzymol.* **1994**, *243*, 203.
(5) Gebhard, M. S.; Deaton, J. C.; Koch, S. A.; Millar, M.; Solomon, E. I. *J. Am. Chem. Soc.* **1990**, *112*, 2217.
(6) Santos, H.; Faraleira, P.; Xavier, A. V.; Chen, L.; Liu, M.-Y.; Le Gall, J. *Biochem. Biophys. Res. Commun.* **1993**, *195*, 551.
(7) Eggink, G.; Engel, H.; Vriend, G.; Terpastra, P.; Witholt, B. *J. Mol. Biol.* **1990**, *212*, 135.
(8) Chen, L.; Sharma, P.; Le Gall, J.; Mariano, A. M.; Teixeira, M.; Xavier, A. V. *Eur. J. Biochem.* **1994**, *226*, 613.
(9) Verhagen, M. F. J. M.; Voorhorst, W. G. B.; Kolkman, J. A.; Wolbert, R. B. G.; Hagen, W. R. *FEBS Lett.* **1993**, *336*, 13.
(10) Archer, M.; Huber, R.; Tavares, P.; Moura, I.; Moura, J. J. G.; Carrondo, M.; Sieker, L. C.; LeGall, J.; Romao, M. J. *J. Mol. Biol.* **1995**, *251*, 690.
(11) Czaja, C.; Litwiller, R.; Tomlinson, A. J.; Naylor, S.; Tavares, P.; LeGall, J.; Moura, J. J. G.; Moura, I.; Rusnak, F. *J. Biol. Chem.* **1995**, *270*, 20273.
(12) Mathieu, I.; Meyer, J.; Moulis, J.-M. *Biochem. J.*, **1992**, *285*, 255.
(13) Eidness, M. K.; O'Dell, J. E.; Kurtz, D. M., Jr.; Robson, R. L.; Scott, R. A. *Protein Eng.* **1992**, *5*, 367.
(14) Petillot, Y.; Forest, E.; Mathieu, I.; Meyer, J.; Moutis, J.-M. *Biochem. J.* **1993**, *296*, 657.
(15) Meyer, J.; Gaillard, J.; Lutz, M. *Biochem. Biophys. Res. Commun.* **1995**, *212*, 827.
(16) Richie, K. A.; Teng, Q.; Elkin, C. J.; Kurtz, D. M., Jr. *Protein Sci.* **1996**, *5*, 883.
(17) Adman, E.; Watenpaugh, K.; Jensen, L. H. *Proc. Natl. Acad. Sci. U.S.A.* **1975**, *72*, 4854.

S0020-1669(95)01653-3 CCC: $12.00 

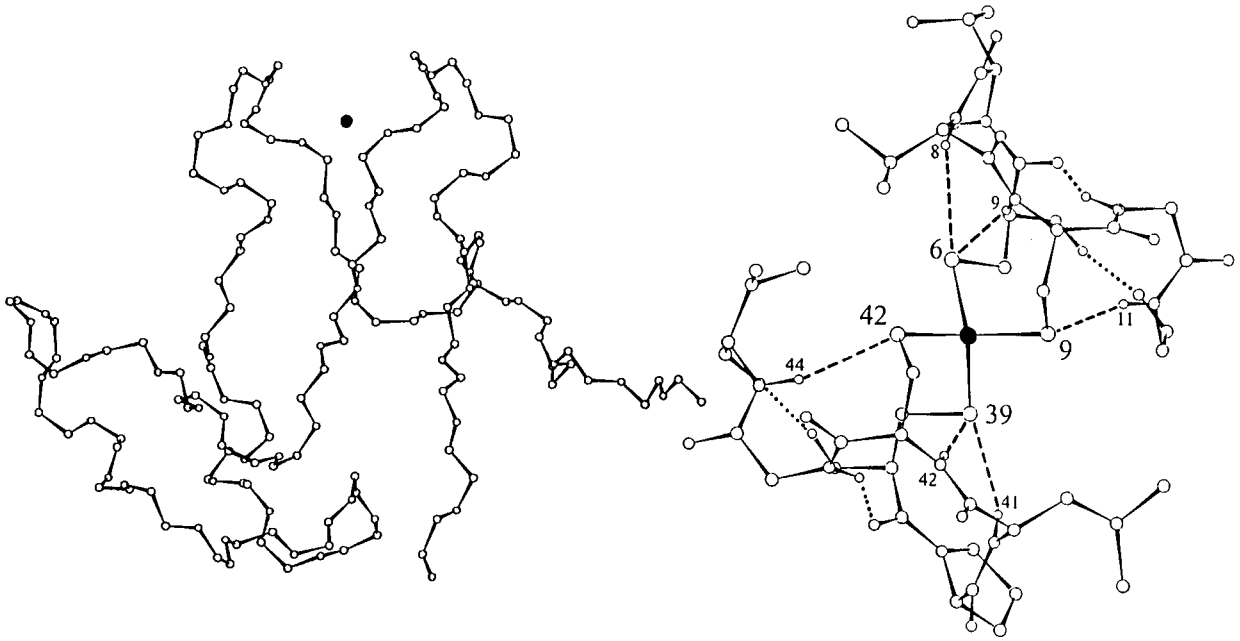


**Figure 1.** (a) Backbone diagram of Rd*Cp*, emphasizing the pseudo-2-fold symmetry in the vicinity of the iron atom. (b) NH···S interactions (---) around the Fe(Cys-*S*)$_4$ center and NH···OC interactions (···) within the chelate loops in Rd*Cp*. In (b), the pseudo-2-fold axis (see text) is perpendicular to the page, passing though the Fe atom. Figures were generated from the coordinates of ref 2: pdb5rxn.ent in the Brookhaven Protein Databank.

**Chart 1.** Rd*Cp*: (a) Partial Sequence; (b) NH···S Interactions

(a)

| | | | | | | | | | | | | | | |
|---|---|---|---|---|---|---|---|---|---|---|---|---|---|---|
| ----- | 5 | 6 | 7 | 8 | 9 | 10 | 11 | ---- | 38 | 39 | 40 | 41 | 42 | 43 | 44 | --------- |
| ----- | T | C | T | V | C | G | Y | ---- | V | C | P | L | C | G | V | --------- |

(b)

| H-bond type[a] | Donor NH | Acceptor S$^\gamma$ |
|---|---|---|
| I | 8/41 | 6/39 |
| III | 9/42 | 6/39 |
| II | 11/44 | 9/42 |

[a] See ref 17.

NMR methods are evolving for the detection of rapidly relaxing protons close to the active sites in functional paramagnetic iron−sulfur proteins.[18−20] Meanwhile, the NH protons involved in the four type I and III interactions detailed above have been detected by $^1$H−$^{113}$Cd and $^1$H−$^{199}$Hg correlation experiments in metal-substituted forms of Rd from *Pyrococcus furiosis.*[21,22] These observations point to the significant covalent character of these NH···S "hydrogen bonds," and this, plus the detection of $^{199}$Hg coupling to alkyl protons of nearby residues,[22] may be relevant to both the tuning of redox potential and a mechanism of electron transfer.

For the type II NH···S interactions involving surface ligands Cys-9 and -42 (Chart 1b; Figure 1b), it has been suggested that a $\beta$-carbon on residue 10 or 43 would destabilize such an interaction by eclipsing the carbonyl oxygen of residue 9 or 42.[17] The presence of conserved Gly residues at positions 10 and 43 is consistent with this idea. Mutation of Gly-10 and -43 may perturb the Rd site and the pattern of NH···S interactions.

This paper reports the production and characterization of mutant Rd*Cp* proteins in which Gly-10 and -43 are mutated to alanine and valine, i.e. substitution of side chain H by $CH_3$ and $CH(CH_3)_2$. Besides the four single mutants, double mutants G10V/G43A and G10V/G43V have been generated and examined.

## Experimental Section

**Materials and Methods.** The enzymes *Pst*I, *Eco*RI, and *Tac* polymerase were obtained from Promega, *Bam*HI from IBI, $T_4$ polynucleotide kinase from NE Biolabs, and calf intestine alkaline phosphatase from Boehringer Mannheim. IPTG, ampicillin, kanamycin, agarose, DNase-free pancreatic RNase, deoxyribonuclease I, and PMSF were all from Sigma. The Sequenase kit was from USB, the Mutagene kit from Bio-Rad, and the expression vector pKK223-3 was from Pharmacia. Bacterial growth media were from Oxoid. The chromatographic column materials used were DE-52 (Whatman), Qiagen-5 (Qiagen), Sephadex G-25/75, and Phenyl Sepharose CL-4B (Pharmacia). The radionucleotide [$\alpha$-$^{35}$S]dATP was purchased from Bresatec. DNA manipulations (plasmid preparations, alkaline lysis, ligations, and transformations) were as described by Sambrook.[23] Oligonucleotides were synthesized on an Applied Biosystems DNA synthesizer Model 380A.

**Oligonucleotides**. Two oligonucleotides were designed from the reported protein and gene sequences.[12,24] A 36-mer (5′-CCC CCC GAA TTC ATG AAG AAG TAT ACA TGT ACA GTA-3′) was complementary to the transcribed strand and included an *Eco*RI cleavage site adjacent to the ATG (start) codon. Although methionine (ATG) is the first amino acid of the Rd*Cp* protein sequence, an additional ATG was

(18) Sadek, M.; Scrofani, S. D. B.; Brownlee, R. T. C.; Wedd, A. G. *J. Chem. Soc., Chem. Commun.* **1995**, 105.
(19) Xia, B.; Westler, M.; Cheng, H.; Meyer, J.; Moulis, J.-M.; Markley, J. L. *J. Am. Chem. Soc.* **1995**, *117*, 5347.
(20) (a) Bertini, I.; Turano, P.; Vila, A. J. *Chem. Rev.* **1993**, *93*, 2833. (b) Chen, Z.; de Ropp, J. S.; Hernandez, G.; La Mar, G. N. *J. Am. Chem, Soc.* **1994**, *116*, 8772.
(21) Blake, P. R.; Park, J.-B.; Adams, M. W. W.; Summers, M. F. *J. Am. Chem. Soc.* **1992**, *114*, 4931.
(22) Blake, P. R.; Lee, B.; Summers, M. F.; Park, J.-B.; Zhou, Z. H.; Adams, M. W. W. *New. J. Chem.* **1994**, *18*, 387.
(23) Sambrook, J.; Fritsch, E. F.; Maniatis, T. *Molecular Cloning: A Laboratory Manual*, 2nd ed.; Cold Spring Harbor Laboratory Press: Cold Spring Harbor, NY, 1989; Vols. 1−3.
(24) Watenpaugh, K. D.; Sieker, L. C.; Herriot, J. R.; Jensen, L. H. *Acta Crystallogr.* **1973**, *B29*, 943.

not included. A 36-mer (5′ -TTC TAT TCG ATA ATT AAC TCC AGG GAC GTC CCC CCC-3′) was complementary to the untranscribed strand between 107 and 130 bases downstream of the last base of the Rd*Cp* nucleotide sequence. A *Pst*I site was included adjacent to the last complementary base for ease of cloning.

**Cloning and DNA Sequencing.** A Rd*Cp* gene fragment was isolated via the polymerase chain reaction[25] using *Cp* chromosomal DNA[26,27] as template. A band at a position consistent with the expected size (316 bp) was detected on a 1% agarose/TBE electrophoresis gel and was the sole product. This product was transferred to NA 45 paper and purified and processed in the normal way. After digestion by restriction enzymes *Eco*RI and *Pst*I, the fragment was inserted into vector pTZ18U and the construct used to transform *E. coli* MV1190. Six ampicillin-resistant colonies were subjected to restriction analysis. Four showed DNA fragments of about 320 bp and were sequenced with the Sequence kit, confirming the presence of the Rd*Cp* gene.

**Mutagenesis.** A Mutagene kit was employed.[28] The plasmid pTZ18U/Rd*Cp* was transformed into *E. coli* CJ236. Single-stranded DNA was isolated and used as template for double-stranded DNA synthesis. The primer used for the G10A/V mutants was 5′-T ATA AAT ATA TG/AC ACA TAC TGT ACA TGT ATA CTT C-3′ while that for the G43A/V mutants was 5′-C TTT TCC TAC TG/AC ACA CAA AGG ACA TAC CCA ATC A-3′. After mutagenesis and identification by sequencing, the four mutants were subcloned into the *Eco*RI and *Pst*I sites of the pKK223-3 vector for protein expression. Single-stranded DNAs containing pTZ18U/Rd*Cp*G43A/V were isolated and used as templates for the production of the G10V/G43A/V double mutants. The sequence of the primer used for the second mutation was 5′-T ATA AAT ATA TAC ACA TAC TGT A-3′. The mismatched base is underlined.

**Protein Expression and Reconstitution.** Plasmids pKK223-3/Rd*Cp* carrying the wild type sequence, the four single mutations (G10A, G10V, G43A, G43V), and the two double mutations (G10V/G43A, G10V/G43V) were transformed into *E. coli* strain JM109. Individual transformants were grown overnight at 37 °C in LB medium containing ampicillin (100 $\mu$g mL$^{-1}$). The following day, 1 L cultures were inoculated with 5 mL of the overnight culture and cells grown at 37 °C with vigorous shaking until $OD_{600}$ reached 1.0−1.2 (ca. 6 h) and induced with isopropyl-$\beta$-D-thiogalactopyranoside (IPTG; 0.4 mM). Following ca. 18 h of additional growth, the cells were harvested by centrifugation for 15 min (7000*g*; 4 °C) and resuspended (3 mL g$^{-1}$) in *E. coli* lysis buffer[23] containing phenylmethanesulfonyl fluoride (PMSF; 133 $\mu$M) and Triton X-100 (0.1%). The cells were lysed by lysozyme (260 $\mu$g mL$^{-1}$). When the lysate became viscous, deoxyribonuclease I (10 $\mu$g mL$^{-1}$) was added and the mixture incubated at 37 °C until the mixture was no longer viscous (ca. 1 h). After centrifugation for 25 min (23000*g*; 4 °C), the supernatant was decanted and added to an equal volume of 50 mM Tris−HCl pH 7.4 (a transient red color may be observed at this step), and the mixture was applied to a DE-52 column (3.3 × 12 cm). Rd was eluted with a 0.10−0.30 M NaCl gradient in 1 L 50 mM Tris−HCl buffer (pH 7.4) at a flow rate of 40 mL h$^{-1}$. For the recombinant Rd and the four single mutants, an intense red band was observed. Fractions with $A_{280}/A_{490} < 6$ were combined and treated with ammonium sulfate to 60% saturation. After the precipitate was discarded, the supernate was applied to a Phenyl Sepharose column (2.8 × 13 cm) equilibrated with 50% saturation ammonium sulfate in 50 mM $KP_i$ buffer, pH 7.5. The red protein was eluted with a 50−0% saturation ammonium sulfate gradient in 1.2 L of 50 mM $KP_i$ buffer, pH 7.5, at a flow rate of 40 mL h$^{-1}$. Fractions with $A_{280}/A_{490} < 2.3$ were pooled and concentrated using an Amicon ultrafiltration cell equipped with a YM3 membrane. Yields were around 20 mg L$^{-1}$ of starting culture for rRd*Cp* and around 10 mg L$^{-1}$ for the four single mutants. For the double mutant G10V/G43A, a pale red band only was observed on the DE-52 column. The same workup followed by two passes through a FPLC Mono-Q anion exchange column provided ca. 2 mg of Fe holoprotein/L of starting culture. The other double mutant G10V/G43V produced no red color on the DE-52 column.

These colorless fractions could be reconstituted readily with iron. The most convenient stage for reconstitution is the crude cell lysate stage. The following procedure was developed from those of ref 29. Protein was precipitated by addition of trichloroacetic acid (20% in water) and mercaptoethanol to final concentrations of ca. 5−10% and 0.3−0.5 M, respectively. After centrifugation, the precipitate was washed with 5% trichloroacetic acid/50 mM mercaptoethanol and redissolved in a minimum of Tris base (0.5 M) containing mercaptoethanol (0.5 M). After removal of insoluble material, the protein was reprecipitated, washed, and redissolved as detailed above. The volume was doubled with Tris−HCl buffer (0.2 M, pH 7), and a 5-fold excess of $Fe(NO_3)_3$ (0.2 M) was added, producing a deep red solution whose color faded with concomitant formation of green insoluble material. After incubation on ice for 1 h, the green precipitate was removed by filtration. After ca. 10-fold dilution with water, the red color reappeared (as the Fe(II) protein was oxidized to Fe(III) by air) and the solution was applied to a DE-52 column. Further purification followed the procedure outlined above.

Under these conditions, recombinant protein, $Fe^{III}$-rRd*Cp*, is obtained at up to 40 mg/L of starting culture. The yields of intact Fe(III) forms of the mutant proteins are 10−20 mg L$^{-1}$.

**Native Rubredoxin.** *Cp* cells were grown in glucose media.[30] Native Rd*Cp* was isolated with a procedure adapted from ref 31. Cells (300 g) were added to 600 mL of KPi buffer (50 mM, pH 7.8) containing lysozyme (300 mg) and DNAase (1.5 mg). The mixture was shaken at 37 °C for 40 min, whereupon RNAase (4 mg) was added. Centrifugation at 10 000 rpm for 30 min, provided a supernatant. Rd*Cp* was isolated with the same approach used for the recombinant protein with an extra step to remove a component of molar mass 12 kDa. Fractions obtained from the hydrophobic chromatography step were pooled and concentrated by ultrafiltration to a volume of about 1 mL. This was applied to an HPLC Superdex 75 16/60 gel filtration column (Pharmacia) equilibrated with KPi (50 mM, pH 7.0) and eluted at 0.75 mL min$^{-1}$. Yields are variable but typically about 5 mg of protein with $A_{280}/A_{490} = 2.2-2.3$.

**Protein Sequencing.** The first 12 amino acids of the recombinant G10A and G10V proteins were confirmed by sequential Edman degradation.

**Electronic Absorption Spectroscopy.** Molar extinction coefficients of the recombinant protein were determined by quantitative drying of a sample of known absorbance in volatile ammonium bicarbonate buffer. Duplicate measurements were made on three independent samples: $\epsilon_{490}$ 6640(70) M$^{-1}$ cm$^{-1}$.

**Metal Stoichiometry.** Metal analysis was carried out using a Plasmaquad inductively coupled plasma mass spectrometer (VG Elemental). Concentrations of protein samples (about 100 $\mu$g in Tris−HCl buffer (10 mM; pH 7.4)) were determined by electronic absorption spectroscopy. The samples were then diluted quantitatively with distilled water and were about 10 $\mu$g mL$^{-1}$ when aspirated into the instrument. The following metals were assayed: $^{55}$Mn, $^{57}$Fe, $^{58}$Ni, $^{59}$Co, $^{63}$Cu, $^{64}$Zn, and $^{111}$Cd. Metal content of the Tris−HCl buffers (iron and zinc, in particular) were less than 10 ppb.

**Electrospray Ionization Mass Spectroscopy.** Spectra were obtained on a VG Bio-Q triple-quadrupole mass spectrometer (VG BioTech, Altrincham, Ches, U.K.). The instrument was tuned and calibrated in the positive ion mode using horse heart myoglobin as the standard and operated in the negative ion mode by inverting the polarity. A mixture of water, methanol, and acetic acid (50/50/1; v/v/v) was used as the mobile phase in the positive mode to facilitate the protonation of the protein molecules while a mobile phase of water, methanol, and ammonia solution or triethylamine (70/30/0.1; v/v/v) was used in the negative ion mode to promote deprotonation. All samples were desalted using a G-25 column (1.2 × 75 cm) in deionized

(25) Saiki, R. K.; Gelfand, D. H.; Stoffel, S.; Scharf, S. J.; Higuchi, R.; Horn, G. T.; Mullis, K. B.; Erlich, H. A. *Science* **1988**, *239*, 487.
(26) Scrofani, S. D. B.; Brereton, P. S.; Hamer, A. M.; Lavery, M. J.; McDowall, S. J.; Vincent, G. A.; Brownlee, R. T. C.; Hoogenraad, N. J.; Sadek, M.; Wedd, A. G. *Biochemistry* **1994**, *33*, 14486.
(27) Brereton, P. S. Ph.D. Thesis, University of Melbourne, 1995.
(28) Kunkel, T. A. *Proc. Natl. Acad. Sci. U.S.A.* **1985**, *82*, 488.
(29) (a) Lovenberg, W.; Williams, W. M. *Biochemistry* **1969**, *8*, 141. (b) Moura, I.; Teixeira, M.; LeGall, J.; Moura, J. J. G. *J. Inorg. Biochem.* **1991**, *44*, 127.
(30) Rabinowitz, J. C. *Methods Enzymol.* **1972**, *24*, 431.
(31) Lovenberg, W.; Sobel, B. E. *Proc. Natl. Acad. Sci. U.S.A.* **1965**, *54*, 193.

water or in 10 mM ammonium acetate and concentrated to 0.2−1.0 mM. The samples were injected directly into the instrument via a Rheodyne injector equipped with a 10 $\mu$L loop and delivered to the vaporization nozzle of the electrospray ion source at a flow rate of 3 $\mu$L min$^{-1}$ via a Phoenix 20 micro LC syringe pump. Nitrogen was used both as a drying gas and for nebulization. All spectra were acquired with the nozzle to skimmer voltage set to 50 V. Final spectra with satisfactory signal-to-noise ratios were obtained over 10−20 scans. The average molar masses were obtained by applying a deconvolution algorithm to the spectra. Theoretical molar mass of apo-Rd was calculated on the basis of the protein sequence from this work. The molar masses of the metalated forms were calculated by adding the atomic mass of $^{56}$Fe minus three protons and assumed atomic masses of $^{65}$Zn and $^{112}$Cd minus two protons, respectively.

**Resonance Raman Spectroscopy.** Excitation lines were provided by a Spectra Physics 2016 Ar ion laser (488 nm) and a Spectra Physics 375 B dye laser using Rhodamine 6G (574 nm). Spectra were recorded using a microscope attached to a Dilor XY confocal raman spectrometer by backscattering directly off the surface of a frozen protein solution. A THMS−600 Linkam temperature-controlled microscope stage was used, which contains a silver block whose temperature is thermostatically controlled by passage of cold nitrogen vapor. Several different protein samples (2−3 mM in 50 mM Tris−HCl buffer, pH 7.4) were applied side by side in ca. 1 $\mu$L droplets to a sapphire disk (7 mm in diameter) placed directly on the silver block so that spectral data could be collected under the same conditions. A glass shroud was placed over the silver block and screwed into position with an O-ring seal. The system was first cooled to −10 °C and the sample cabinet flushed with dinitrogen for ca. 2 min to remove dioxygen. The system was then cooled to −180 °C, a temperature chosen to eliminate any potential condensation of trace $O_2$. A typical integration time of 100 s was applied to each spectrum at laser power levels of ca. 40−100 mW. No protein damage was observed under these conditions. Improvements in the signal-to-noise ratio were achieved by averaging 3−10 spectra collected by focusing the laser on different sites of the same droplet. No smoothing function was applied to the data. Spectral bands obtained using the Ar laser were calibrated with characteristic plasma lines and were accurate to $\pm$1.0 cm$^{-1}$. Band positions were steady to $\pm$0.5 cm$^{-1}$ with the Ar laser during data collection but shifted slightly with the dye laser due to frequency drift of the exciting line. Thus, each spectrum obtained with the dye laser was calibrated against those obtained with the Ar laser before being averaged. A typical spectral band-pass was 2.7 cm$^{-1}$.

**Electrochemistry.** Square-wave voltammetry[32] was carried out at 25 $\pm$ 0.5 °C using a standard three-electrode configuration on a Cypress CS−1087 instrument. The working electrode was a pyrolytic graphite electrode modified by poly(L-lysine). The modification was achieved by dipping the electrode into a 10 mM poly(L-lysine) solution for 2 min, followed by rinsing carefully with deionized water. A platinum wire acted as the auxiliary electrode. Reduction potentials were measured relative to a KCl-saturated Ag/AgCl reference electrode ($E°$ = 199 mV *vs* SHE at 25 °C) and reported versus SHE. The potentials were determined directly from the current peak potentials of the voltammograms. The number of electrons ($n$) transferred was determined from the width at half-height (126 mV/$n$). Rd*Cp* samples (50−100 $\mu$M) were dissolved in 30 mM Tris−HCl, pH 7.4, containing 0.1 M NaCl.

**NMR of $^{113}$Cd-Substituted Samples.** The recombinant and G10V, G43V, and G10V/G43V proteins were chosen for $^{113}$Cd substitution and NMR investigations. The procedure employed purified Fe(III) forms and followed the reconstitution procedure outlined above except that 2 equiv of $^{113}$Cd(NO$_3$)$_2$ (20 mM) was used. After incubation on ice for 1 h, the mixture was loaded onto a DE-52 column (1.6 × 4 cm). After washing with ca. 10 column volumes of 20 mM Tris−HCl buffer (pH 7.0) to remove excess Cd(NO$_3$)$_2$ and another 5 column volumes of 20 mM KPi (pH, 6.8) to change buffer, the proteins were eluted with a 0.1−0.4 M NaCl gradient in the same buffer (120 mL). The sample solution was concentrated to ca. 0.45 mL, and 0.05 mL of $^2$H$_2$O was added for signal lock, leaving final conditions of 20 mM KPi (pH 6.8), and 200 mM NaCl in 90% H$_2$O/D$_2$O. The samples (4−6 mM) were sealed anaerobically into an NMR tube for subsequent investigations.

**Table 1.** Metal Content of Rd*Cp*[a]

| protein | Fe | Zn |
|---|---|---|
| native | 0.94(1) | 0.05(1) |
| recombinant | 1.01(1) | 0.02(1) |
| G10A | 1.01(1) | 0.03(1) |
| G10V | 1.12(2) | 0.04(1) |
| G43A | 0.99(3) | 0.01(1) |
| G43V | 1.02(1) | 0.01(1) |
| G10V/G43A[b] | n.d. | 1.3(1) |
| G10V/G43A[c] | 0.89(3) | n.d. |
| G10V/G43V[c] | 0.84(6) | n.d. |

[a] Metal/protein molar ratio: single-standard deviations are quoted in parentheses; n.d. = not detected. [b] As isolated (see text). [c] After reconstitution with iron (see text).

All $^1$H NMR experiments were recorded at 303 K on a Bruker DRX500 spectrometer operating at 500.13 MHz. Two-dimensional phase-sensitive homonuclear spectra were acquired with simultaneous acquisition in the $\omega_2$ dimension, and States-TPPI[33] was employed for quadrature detection in the $\omega_1$ dimension. NOESY[34] and TOCSY[35] experiments were recorded with spectral widths of 8013 Hz in both dimensions and 64−128 transients for each 512−768 $\omega_1$ increment. The water signal was suppressed with low-power irradiation for 0.5−1.0 s during the relaxation delay. NOESY (100−250 ms) spectra were acquired with additional water presaturation during the mixing time. TOCSY (40−90 ms) spectra were acquired using the MLEV-17 mixing scheme, flanked by 2.5 ms trim pulses.

NOESY and TOCSY data either were processed using Bruker XWIN-NMR software or were converted to a suitable format for processing with Varian VNMR 5.1 software. Typically, 60−80° shifted square sine bells were used in both dimensions and zero-filled to a final matrix size of 2048 × 2048 real data points. $^1$H chemical shifts were referenced to the H$_2$O signal at 4.73 ppm (303 K).

$^{113}$Cd NMR spectra were acquired on a Bruker DRX500 NMR spectrometer (110.92 MHz for $^{113}$Cd). $^{113}$Cd resonances were referenced indirectly to Cd(ClO$_4$)$_2$ (0.0 ppm, 0.1 M in H$_2$O).

## Results and Discussion

**Characterization of Recombinant and Mutant Proteins.** The Rd*Cp* gene has been cloned previously and the recombinant protein expressed in *E. coli* as a mixture of forms containing the native Fe(III) metal and Zn(II).[12] In contrast to the case of the native protein,[1] the N terminus was not formylated in either recombinant form. The protein sequence was shown[12] to vary from the previously reported sequence[24] in that asparagine is present at positions 14 and 22 and glutamine at position 48 rather than the corresponding acids.

The present work confirms that sequence and reports high-yield expression (40 mg (L of starting culture)$^{-1}$) of nonformylated recombinant protein via the pKK223−3/JM109 system after reconstitution of the accompanying Zn(II) forms with Fe(III) (Tables 1 and 2). The reconstitution can be effected at the crude lysate stage of the isolation. Equivalent procedures lead to yields of ca.10−20 mg L$^{-1}$ for the six Fe(III) mutant proteins G10A, G10V, G43A, G43V, G10V/G43A, and G10V/G43V.

The double mutants are expressed essentially as the Zn(II) forms (Table 2). It is interesting to note that a synthetic gene based on the previously reported sequence also expressed in *E.*

(32) (a) Armstrong, F. A.; Hill, H. A. O.; Oliver, B. N.; Walton, N. J. *J. Am. Chem. Soc.* **1984**, *106*, 921. (b) Smith, E. T.; Feinberg, B. A. *J. Biol. Chem.* **1990**, *265*, 14371.

(33) Marion, D.; Ikura, M.; Tschudin, R.; Bax, A. *J. Magn. Reson.* **1989**, *85*, 393.

(34) Macura, S.; Ernst, R. R. *Mol. Phys.* **1980**, *41*, 95.

(35) Bax, A.; Davis, D. G. *J. Magn. Reson.* **1985**, *65*, 355.

**Table 2.** Molar Masses (Da) Determined by Electrospray Mass Spectrometry[a]

| Rd*Cp* | calcd | found[b] |
|---|---|---|
| native | 6047.6[c,d] | 6047(1)[f] |
| | 6075.6[c,e] | 6075(1)[f] |
| | 6100.5[d] | 6100(1) |
| | 6128.5[e] | 6129(1) |
| recombinant | 6100.5 | 6101(1) |
| $Zn^{II}$-recombinant[g] | 6110.0 | 6111(1) |
| G10A | 6114.5 | 6115(1) |
| $Zn^{II}$-G10V[g] | 6153.0 | 6152(1) |
| G10V | 6142.5 | 6143(1) |
| G43A | 6114.5 | 6115(1) |
| G43V | 6142.5 | 6143(1) |
| $Zn^{II}$-G10V/G43A[g] | 6167.0 | 6167(1) |
| G10V/G43A | 6156.5 | 6157(1) |
| G10V/G43V | 6184.5 | 6185(1) |
| $^{113}Cd^{II}$-recombinant | 6158.7 | 6159(1) |
| $^{113}Cd^{II}$-G10V/G43V | 6242.7 | 6244(1) |

[a] Determined under basic conditions in the negative-ion mode unless otherwise stated (see text). [b] Single-standard deviations given in parentheses. [c] Apoprotein. [d] Unformylated N terminus. [e] Formylated N terminus. [f] Determined under acid conditions in the positive-ion mode. [g] Colorless Zn form as isolated: see text.

*coli* with high proportions of the Zn(II) form.[13] This sequence features triple mutation at positions 14 (N → D), 22 (N → D) and 48 (Q → E) with a consequent change in charge of −3 for the protein at pH 7. Substitution of zinc for iron has been observed for other iron proteins expressed in *E. coli*, including one only of the two Fe(Cys-*S*)$_4$ sites in desulforedoxin from *D. gigas*.[11,36]

The identity of these proteins was confirmed by N-terminal sequencing for the recombinant, G10A and G10V forms, by metal analysis (Table 1) and by electrospray ionization mass spectrometry (Table 2). When analysis was performed under acid conditions, metal ion was found to be released readily into solution and apoprotein ions only were detected in positive ion mass spectra. However, for the recombinant and mutant proteins measured under basic conditions in the negative ion mode,[14] holoprotein ions only were detected (Figure 2) at masses expected for unformylated Fe(III) and Zn(II) forms. The native protein, as isolated in the present work, is a mixture of formylated and unformylated forms.[1] A number of weak protein ion peaks are seen to higher mass numbers. Their relative intensities and *m*/*e* values vary with the composition of the protein buffer and the mobile phase. These peaks are due to the formation of $Na^+$− and/or $NH_4^+$−protein adducts. The six mutant proteins are much less stable under acidic conditions than are the native and recombinant forms. In 10% trichloroacetic acid, the mutant proteins decolor and precipitate completely in less than 5 min compared to at least 1 h for the native and recombinant forms.

**Structural Aspects.** The chelate loops C6−Y11 and C39−V44 each contain six residues and determine the pseudo-2-fold symmetry of the Fe(Cys-*S*)$_4$ site of Rd*Cp* (Scheme 1; Figure 1). Besides the three NH···S interactions in each loop, two hydrogen bonds, characteristic of an antiparallel $\beta$ sheet, help maintain the tight turn: one connects the ends of each loop (C6−NH···OC−Y11; C39−NH···OC−V44) and the other reaches across each loop (G10−NH···OC−C6 ; C43−NH···OC−C39) (Table 3; Figures 1 and 3). The two bonds in loop C6−Y11 can be seen clearly in Figure 3a,b (in the latter, the residues are identified at the C$^\alpha$H atom). The equivalent view of the C39−NH···OC−V44 bond in loop C39−V44 is obstructed in Figure 3d: the C39−NH···OC−V44 bond lies beneath the side chain of V38. Note that C6 and C39 are each involved in four hydrogen bonds. Each loop defines a shallow pocket in the surface of the molecule: the amide CO groups not involved in hydrogen bonding (7−10, 40−43) help define this pocket.

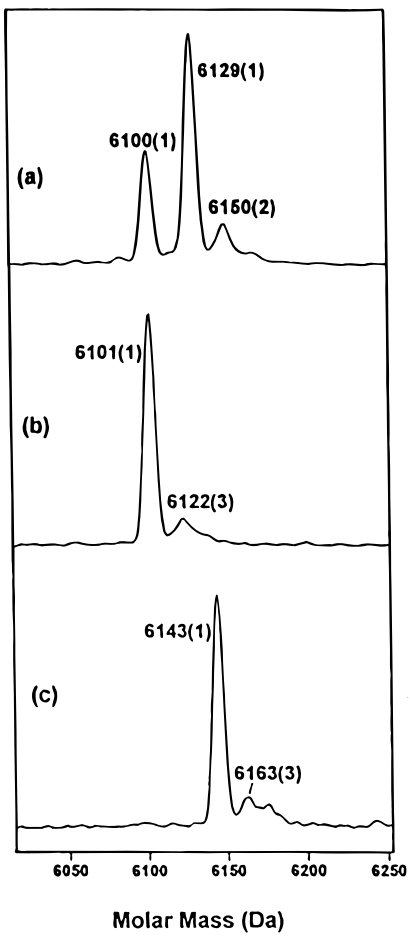


**Figure 2.** Negative-ion electrospray ionization mass spectra. The proteins (0.2−1.0 mM) suspended in distilled water or 10 mM ammonium acetate were infused into a mixture of MeOH/$H_2O$/$NH_3$-(aq) or $Et_3N$ (30/70/0.1 v/v/v). (a) native; (b) recombinant; (c) G10V. Weak peaks with higher molar masses are due to the formation of $Na^+$− and/or $NH_4^+$−protein adducts.

**Table 3.** Hydrogen Bonds in the Chelate Loops

| residue | NH donor to | CO acceptor from[a] | S acceptor from |
|---|---|---|---|
| C6 | OC−Y11 | G10−NH | V8−NH |
| | | | C9−NH |
| T7 | OC−Q48 | surface | |
| V8 | S$^\gamma$-C6 | surface | |
| C9 | S$^\gamma$-C6 | surface | Y11−NH |
| G10 | OC−C6 | surface | |
| Y11 | S$^\gamma$-C9 | C6−NH | |
| C39 | OC−V44 | G43−NH | L41−NH |
| | | | C42−NH |
| P40 | | surface | |
| L41 | S$^\gamma$-C39 | surface | |
| C42 | S$^\gamma$-C39 | surface | V44−NH |
| G43 | OC−C39 | surface | |
| V44 | S$^\gamma$-C42 | C39−NH | |

[a] "Surface" indicates that this CO group is part of the exterior surface of Rd*Cp*.

(36) Mann, G. J.; Graslund, A.; Ochai, E.-I.; Ingamarson, R.; Thelander, L. *Biochemistry* **1991**, *30*, 1939.
(37) Yang, S.-S.; Ljungdahl, L. C.; Dervartanian, D. V.; Watt, G. D. *Biochim. Biophys. Acta* **1980**, *590*, 24.
(38) Lee, W.-Y.; Brune, D. X.; LoBrutto, R.; Blankenship *Arch. Biochem. Biophys.* **1995**, *318*, 80.

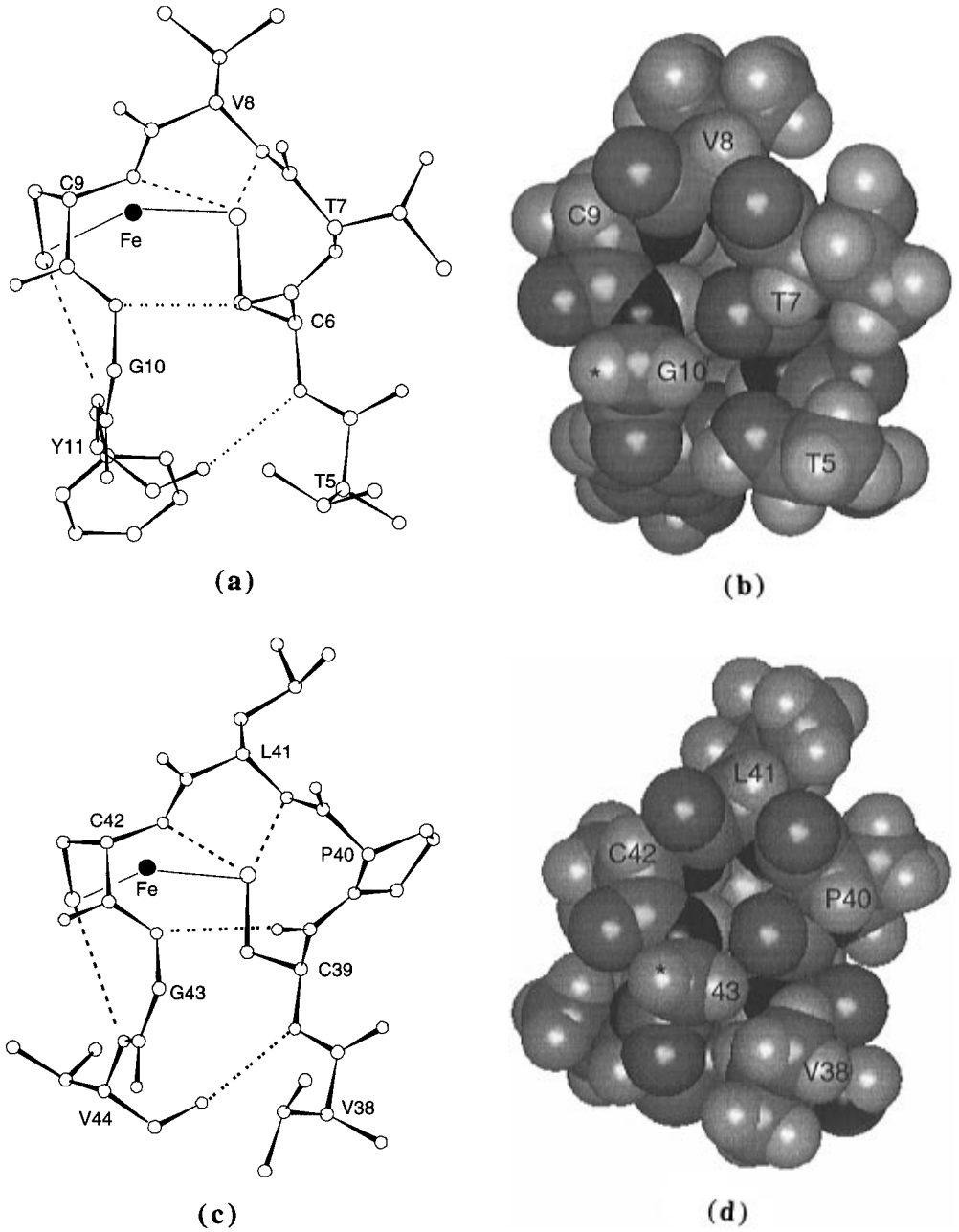


**Figure 3.** Structure around the chelate loops of Cd-rRd*Cp* (generated from coordinates supplied by the authors of ref 39). Loop T5−Y11: (a) ball-and-stick model; (b) space-filling model. Loop V38−V44: (c) ball-and-stick model; (d) space-filling model. Hydrogen atoms are absent in (a) and (c). Individual amino acid residues are identified at $C^{\alpha}$ in (a) and (c) and at $H^{\alpha 1}$ in (b) and (d), except for T5, V38, and V44, which are labeled at a $H^{\gamma}$ atom. The points of mutation at the G10 and G43 $H^{\alpha 2}$ atoms are indicated by an asterisk.

The crystal structure of the Cd(II)-substituted form of the recombinant protein Cd-rRd*Cp* has been solved.[39] The overall structure is similar to that of the native protein,[2,4] but there are differences in and around the active site. These are outlined briefly here to assist interpretation of $^1$H NMR spectra. The four Cd−S distances are the same, within error, at the present stage of refinement. The mean value of 2.58(5) Å is 0.29(6) Å longer than the Fe−S bonds in Rd*Cp*.[4] Table 4 lists changes in hydrogen-bonding distances for the chelate loops. The four NH···S distances to the buried ligands C6 and C39 decrease by 0.17−0.28(6) Å in response to the expansion of the $MS_4$ core. Those to surface ligands C9 and C42 differ in their response: the distance Y11−NH···S−C9 decreases by 0.12 Å but V44−NH···S−C42 has not changed significantly. The latter

(39) Lavery, M. L.; Guss, M. Unpublished observations. The nominal resolution limit on the data is 1.5 Å. At the present stage of refinement, the *R* factor is 0.167 for all data from 7 to 1.5 Å.

**Table 4.** Differences in Hydrogen-Bonding Distances in $Fe^{III}$-Rd[a] and $Cd^{II}$-Rd[b]

| bond | $\Delta r$ (Å)[c] |
|---|---|
| C6−NH···OC−Y11 | −0.02 |
| C39−NH···OC−V44 | +0.04 |
| G10−NH···OC−C6 | +0.07 |
| G43−NH···OC−C39 | +0.14 |
| V8−NH···S−C6 | −0.28 |
| C9−NH···S−C6 | −0.24 |
| L41−NH···S−C39 | −0.28 |
| C42V8−NH···S−C39 | −0.17 |
| Y11−NH···S−C9 | −0.12 |
| V44−NH···S−42 | +0.06 |

[a] Reference 4. [b] Reference 39. [c] Change in H···X distance (X = O, S) assuming *r*(NH) = 1.03 Å: a positive value indicates an increase in the Cd protein relative to the Fe protein. Standard deviation 0.06 Å.

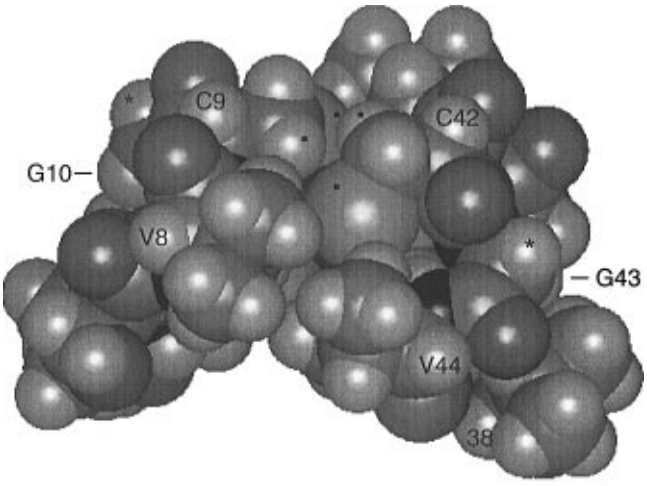


**Figure 4.** Partial structure of Cd-rRd*Cp* around the active site. Residues are numbered at $H^{\alpha 1}$ atoms. The view is approximately perpendicular to those of Figure 3. The hydrophobic contacts between loops 5−11 and 38−44 are apparent. The points of mutation at the G10 and G43 $H^{\alpha 2}$ atoms are indicated by an asterisk. The C9 and C42 $H^{\beta 2}$ and $S^{\gamma}$ atoms are identified by black dots.

behavior can be traced to the effect of nonbonded interactions between the $H_3C^{\gamma}$ groups of the isopropyl side chains of V44 and V8 and the S ligand atoms of C6 and C42 (Figure 4). $H_3C^{\gamma 1}$−V44 contacts $H_3C^{\gamma 1,2}$−V8 as well as S−C42 while $H_3C^{\gamma 2}$−V44 contacts $H_3C^{\gamma 2}$−V8, $H_2C^{\beta}$−V8, and S−C6. In contrast to the buried residues, the surface side chains of V8 and V44 are able to adjust to the core expansion. The nonbonded interactions mean that V44−NH alters position, and in contrast to the other NH···S interactions, the V44−NH···S−C42 distance is not compressed.

**Nuclear Magnetic Resonance.** Effective substitution of diamagnetic Cd(II) for paramagnetic Fe(III) was confirmed for the recombinant and G10V/G43V proteins by mass spectrometry (Table 2). In addition, single resonances were observed at the following chemical shifts in $^{113}$Cd NMR spectra of $^{113}$Cd-substituted proteins: recombinant, 729.4; G10V, 716.1; G43V, 725.5; G10V/G43V, 717.0 ppm.

The $^1$H NMR spectrum of $^{113}Cd^{II}$-rRd*Cp* has been assigned.[40] A comparison of amide $^1$H chemical shifts with those of the $Cd^{II}$-substituted G10V, G43V and G10V/G43V proteins is made in Table 5. The fingerprint regions of 2D TOCSY spectra for the recombinant and G10V/G43V proteins are shown in Figure 5. Structural changes induced by the mutations appear to be highly localized. The sums of the chemical shift changes for a given resonance in the single mutants correlate closely with the observed shift change in the double mutant (Table 5). To first order, the covalently bound Cd(Cys-*S*)$_4$ center does not transmit the magnetic changes induced by the mutations from one chelate loop to the other. The localization is also consistent with the weak hydrophobic contacts which exist between the chelate loops (Figure 4; but *vide infra*).

In the G10V mutant, large shift changes are observed for the NH protons of the C6−Y11 loop (Table 5). This correlates with the $Pr^i$ side chain of V10 occupying part of the surface pocket defined by the loop. The C6−Y11 NH functions line the bottom of the pocket (Figure 3b). The significant shift changes also observed for I12 and Y13 NH protons may be associated with their proximity to the Y11 aromatic ring.

The observations for the C39−Y44 loop in G43V are very different. A single dominant shift change of −0.36 ppm is seen for the V44−NH proton with small changes (<0.06 ppm) for the other members of the loop (Table 5). Examination of the $Cd^{II}$-rRd*Cp* structure reveals that the side chain of V38 may block an orientation of the V43 side chain equivalent to that discussed above for V10 in the G10V mutant (Figure 3d and 4). The V43 side chain would experience nonbonded repulsions from both OC−C42 and $H_3C^{\gamma 1}$-V38. An alternative orientation between the 42 and 43 OC functions would impose nonbonded repulsions with OC−C42 and $H_3C^{\gamma 1}$−V44 (Figure 3d and 4). These are just the residues involved in the V44−NH···S−C42 interaction whose NH function exhibits the dominant chemical shift change and which, as discussed above, was structurally sensitive to the incorporation of cadmium.

This difference in preferred orientation appears to be driven by differences in the molecular surface presented by the two chelate loops. For the G10V mutant, the orientation of the V10 side chain into the loop pocket is favored as the side chain of T5 is swung away from the pocket due to the interaction of $HO^{\gamma}$−T5 with the C6−NH···OC−Y11 hydrogen bond (Figure 3a,b). Such an interaction is not possible for V38, the residue in the equivalent position in the G43V mutant, and its side chain adopts a different orientation. In particular, its $H_3C^{\gamma 1}$ group protrudes into the C39−V44 chelate loop pocket (Figures 3c,d and 4), apparently disfavoring occupation by the V43 side chain.

Two significant shift changes are seen in the nonmutated loops: G10V: V44, 0.29 ppm. G43V: Y11, 0.11 ppm (Table 5). Y11 and V44 are related by the pseudo symmetry, as are C9 and C42. These perturbations appear to be propagated via the close contacts between C9 and C42 $H^{\beta 2}$ and $S^{\gamma}$ atoms. A C9 $H^{\beta 2}$···$H^{\beta 2}$−C42 close contact of 2.29 Å in native Rd*Cp* (van der Waals distance 2.4−2.9 Å) has increased to 2.46 Å in Cd-rRd*Cp*, but C9−$H^{\beta 2}$···S−C42 has decreased significantly from 3.28 to 3.05 Å (van der Waals distance 3.2−3.45 Å). In the G10V mutant, the effect of the structural change can be communicated via the C9−$H^{\beta 2}$···C42−$H^{\beta 2}$ and/or C9−$H^{\beta 2}$···S−C42 contacts to the V44−NH···S−C42 interaction (Figure 4), leading to the observed chemical shift change in V44−NH. In the G43V mutant, it can be communicated similarly to the Y11−NH···S−C9 interaction.

**Table 5.** $^1$H Chemical Shifts $\delta$ (ppm) for NH Protons in the Loops 6−13 and 38−46 of $^{113}$Cd-substituted Rd*Cp* Proteins[a]

| | | change in $\delta$[b] | | | |
|---|---|---|---|---|---|
| residue | $\delta$ recombinant | G10V | G43V | G10V/G43V | predicted[c] |
| C6 | 9.19 | −0.76 | −0.04 | −0.79 | −0.80 |
| T7 | 8.39 | −0.66 | 0.00 | −0.71 | −0.66 |
| V8 | 9.41 | 0.59 | 0.05 | 0.60 | 0.64 |
| C9 | 9.35 | 0.02 | 0.04 | 0.09 | 0.06 |
| G10 (V10) | 7.82 | −0.72 | 0.01 | −0.69 | −0.71 |
| Y11 | 8.97 | 0.37 | 0.11 | 0.41 | 0.48 |
| I12 | 7.38 | −0.56 | 0.00 | −0.58 | −0.56 |
| Y13 | 9.45 | 0.22 | 0.01 | 0.22 | 0.23 |
| V38 | 6.43 | −0.07 | −0.02 | −0.10 | −0.09 |
| C39 | 8.84 | −0.01 | −0.09 | −0.15 | −0.10 |
| P40 | | | | | |
| L41 | 8.91 | 0.04 | 0.05 | 0.09 | 0.09 |
| C42 | 8.74 | 0.11 | −0.06 | 0.05 | 0.05 |
| G43 (V43) | 7.95 | 0.01 | −0.04 | −0.06 | −0.03 |
| V44 | 7.95 | 0.29 | −0.36 | −0.03 | −0.07 |
| G45 | 8.19 | −0.06 | −0.04 | −0.13 | −0.10 |
| K46 | 8.39 | −0.07 | −0.02 | −0.19 | −0.09 |

[a] Chemical shifts measured in phosphate buffer (20 mM; pH 6.8), 0.2 M NaCl at 303 K referred to $^1H_2O$ at 4.73 ppm. Error ±0.02 ppm. [b] The difference between the recombinant and mutated proteins. Positive shifts are downfield. Error ±0.04 ppm. Residues are listed only if they show a shift change of 0.04 ppm or more in at least one of the mutant proteins listed. [c] The sum of the experimental changes in $\delta$ observed for G10V and G43V.

(40) Scrofani, S. D. B. Unpublished observations.

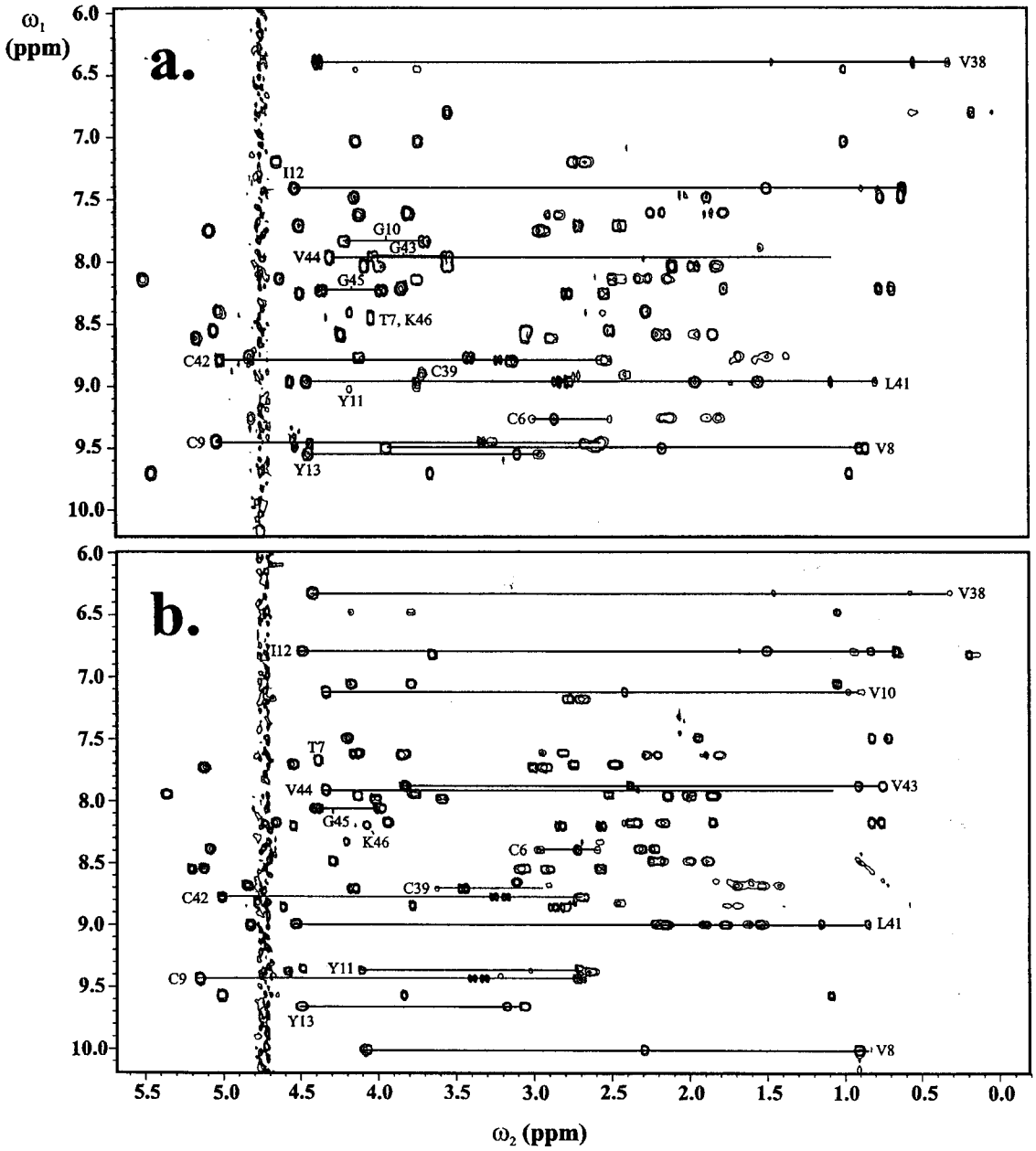


**Figure 5.** Fingerprint region of the 500 MHz TOCSY (90 ms) spectra of $^{113}$Cd-substituted Rd*Cp* proteins: (a) recombinant; (b) G10V/G43V mutant. Conditions: concentration, 5 mM; buffer, potassium phosphate (20 mM; pH 6.8), NaCl (200 mM); *T*, 303 K. Spin systems for residues 6−13 and 38−46 only are identified.

**Electronic Spectra.** Spectra of the native,[31] recombinant, and mutant forms are essentially indistinguishable. Absorbance ratios $A_{280}/A_{490}$ and $A_{280}/A_{380}$ of 2.3 and 2.0, respectively, were observed for highly purified samples of each mutant. The molar extinction coefficient at 490 nm for the recombinant protein was determined to be 6640(70) $M^{-1}$ $cm^{-1}$ in 10 mM ammonium bicarbonate. This value is similar to those reported for a number of other Rds.[37,38] An anomalously high value has been reported previously for native Rd*Cp* ($\epsilon_{490}$ = 8850 $M^{-1}$ $cm^{-1}$).[1,31] The present value was used to estimate protein concentrations for metal analysis (Table 1).

Detailed comparison of solution spectra of the mutants reveals that the long wavelength shoulder ($S_\sigma \rightarrow Fe_{\sigma^*}$)[5] of the native and recombinant forms experiences a small red shift: a maximum at ca. 570 nm is observed in all six mutants (Figure 6). The weak absorbance at ca. 750 nm ($S_\pi \rightarrow Fe_{\pi^*}$)[5] is sensitive to the mutations at G10 (red shift of 7 nm for G10A and 15 nm for G10V) but not to those at G43 (Figure 6). The behavior of the double mutants is determined by the mutation at G10.

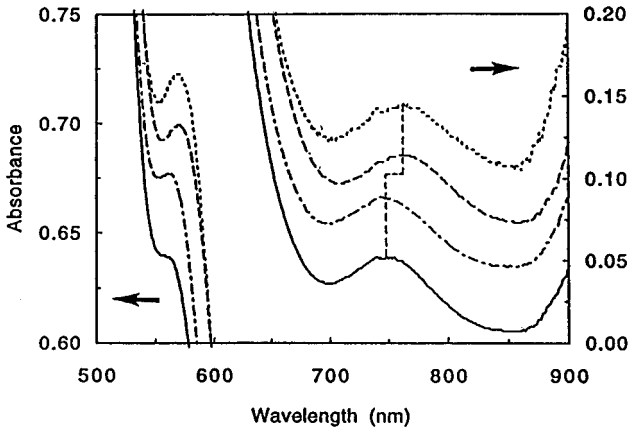


**Figure 6.** Electronic absorption spectra of oxidized Rd*Cp* proteins (0.41 mM in 50 mM Tris−HCl (pH, 7.4)): recombinant (—); G43V (—·—); G10V (– –); G10V/G43V mutant (···). The spectra have been offset by 0.03 absorption unit for clarity.

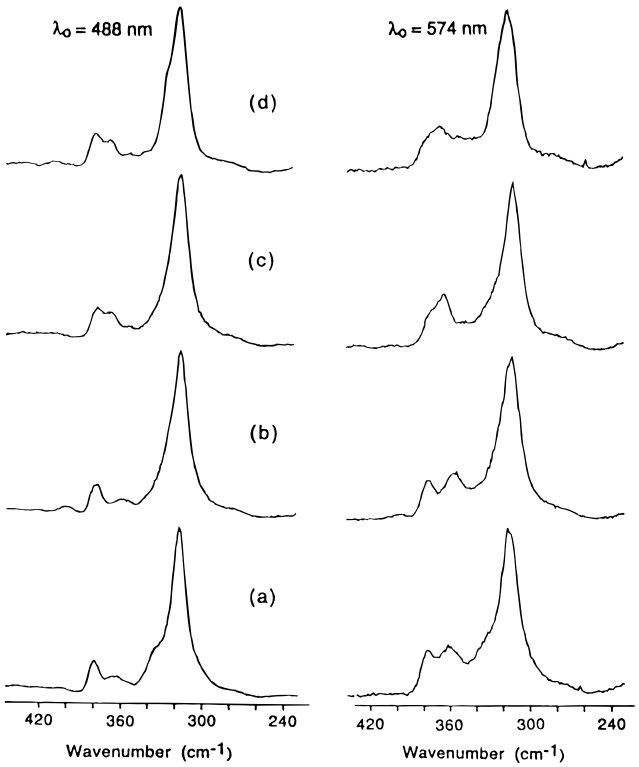


**Figure 7.** Resonance Raman spectra of oxidized Rd*Cp* proteins obtained at 93 K: (a) recombinant; (b) G43V; (c) G10V; (d) G10V/G43V.

**Table 6.** Selected Resonance Raman Data ($cm^{-1}$) for Rd*Cp* Proteins

| protein | $\nu_1$[a] | $\nu_{3a}$[a] | $\nu_{3b,c}$[b] | $\nu_{3a} - \nu_{3b,c}$ |
|---|---|---|---|---|
| native | 316 | 378 | 362 | 16 |
| recombinant | 316 | 379 | 361 | 18 |
| G10A | 315 | 378 | 366 | 12 |
| G10V | 314 | 377 | 366 | 11 |
| G43A | 315 | 380 | 358 | 22 |
| G43V | 315 | 380 | 358 | 22 |
| G10V/G43A | 316 | 379 | 367 | 12 |
| G10V/G43V | 316 | 378 | 367 | 12 |

[a] Data with 488 nm laser excitation. [b] Data with 574 nm laser excitation and calibration against $\nu_1$ defined by the data with 488 nm excitation.

**Resonance Raman Spectroscopy.** Spectra of recombinant protein and a selection of mutant forms are shown in Figure 7. Data are listed in Table 6. They indicate the presence of an intact $FeS_4$ center in each protein.[41−43] The spectra of the native and the recombinant proteins are indistinguishable.[13] They are dominated by the strong band at 316 $cm^{-1}$, assigned to the totally symmetric breathing mode of the $FeS_4$ center, $\nu_1(A_1)$. The asymmetric stretching mode which is triply degenerate in $T_d$ symmetry, $\nu_3(T_2)$, is enhanced when the laser line is tuned to longer wavelength at 574 nm (Figure 7). It is present as two components, $\nu_{3a}$ and $\nu_{3b,c}$ at 379 and 361 $cm^{-1}$, respectively. The broad feature of the second component is consistent with overlap of $\nu_{3b}$ and $\nu_{3c}$. This contrasts with the spectrum of the Rd from *D. gigas*, in which the three components of $\nu_3$ are resolved.[42] The splitting of $\nu_3$ indicates a point symmetry less than $T_d$ and/or coupling to other vibrational modes in the same frequency region.[41−43] The X-ray crystal structure of Rd*Cp* indicates effective $D_{2d}$ local point symmetry for the $FeS_4$ group.[4]

**Table 7.** Midpoint Potentials *E* (mV) for Rd*Cp* Proteins[a]

| protein | *E* | $\Delta E$[b] | predicted[c] |
|---|---|---|---|
| native | −76 | | |
| recombinant | −77 | | |
| G10A | −104 | −27 | |
| G10V | −119 | −42 | |
| G43A | −93 | −16 | |
| G43V | −123 | −46 | |
| G10V/G43A | −134 | −57 | −58 |
| G10V/G43V | −163 | −86 | −88 |

[a] Determined by square-wave voltammetry, *vs* SHE. [b] $E_{mutant} - E_{recombinant}$. [c] Sum of observed $\Delta E$ for the proteins mutated at individual single sites.

The overall spectral patterns of the mutants are similar to that of the recombinant protein (Figure 7). $\nu_1(A_1)$ is seen at 315 ± 1 $cm^{-1}$, indicating that the Fe−S bond strength is essentially unaffected by these mutations. However, the pattern of the $\nu_3$ components, a sensitive indicator of local symmetry, varies. Mutation at G10 decreases the separation between $\nu_{3a}$ and $\nu_{3b,c}$ (Figure 7, Table 6). In contrast, mutation at G43 results in a slightly larger separation of $\nu_{3a}$ and $\nu_{3b,c}$, mainly due to a small shift of the $\nu_{3b,c}$ component to lower energy. For the double mutants, the structure of the $\nu_3$ mode is similar to that seen in the G10 mutants.

**Electrochemistry.** Square-wave voltammetry (SWV) was carried out at a pyrolytic graphite edge electrode using poly(L-lysine) as the electron transfer promotor. Results are given in Table 7 and Figure 8. Electron transfer between the electrode and Rd*Cp* is promoted efficiently by poly(L-lysine), and electrochemistry is reversible under all conditions: the peak potentials remain constant at different pulse frequencies and a plot of the peak currents versus the square roots of those frequencies is linear (Figure 8). This is a one-electron couple, $Fe^{III}/Fe^{II}$, as characterized by the observed peak width at half-height of 127 ± 1 mV.[32] However, the observed peak potentials depend upon the poly(L-lysine) concentration in solution and shift significantly in the positive direction with increasing poly(L-lysine) concentration.[44] In order to define the relative reduction potentials of the various forms of rubredoxin under the same conditions, a poly(L-lysine)-modified working electrode was used (see Experimental Section).

The observed midpoint potentials of the native and recombinant Rd*Cp* are the same within experimental error (−76(2) mV versus SHE) and consistent with a previously reported value (−74 mV) also estimated by SWV.[32] The values for the six mutants are more negative than that of the recombinant form (Table 7); i.e., the oxidized state has been stabilized relative to the reduced one. Substitution of glycine by valine has a larger effect than substitution by alanine. Interestingly, turning on four NH···S interactions in a model $[Fe^{II}(SR)_4]^{2-}$ complex induced a positive shift of 240 mV, while exposing similar centers to more polar environments also caused positive shifts.[45,46] However, it is proposed that a combination of the detailed orientation of peptide amide dipoles, access to solvent water, and the presence of NH···S interactions modulates redox potentals in iron−sulfur proteins.[47−50] The specific effect of the present

(41) Yachandra, V. K.; Hare, J.; Moura, I.; Spiro, T. G. *J. Am. Chem. Soc.* **1983**, *105*, 6455.
(42) Czernuszewicz, R. S.; LeGall, J.; Moura, I.; Spiro, T. G. *Inorg. Chem.* **1986**, *25*, 696.
(43) Czernuszewicz, R. S.; Kilpatrick, L. K.; Koch, S. A.; Spiro, T. G. *J. Am. Chem. Soc.* **1994**, *116*, 7134.
(44) Xiao, Z.; Lavery, M. J.; Bond, A. M.; Wedd, A. G. Submitted for publication in *J. Biol. Inorg. Chem.*
(45) Nakata, M.; Ueyama, N.; Fuji, M.-A.; Nakamura, A.; Wada, K.; Matsubara, H. *Biochim. Biophys. Acta* **1984**, *788*, 306.
(46) Ueyama, N.; Okamura, T.; Nakamura, A. *J. Chem. Soc., Chem. Commun.* **1992**, 1019.
(47) Jensen, G. M.; Warshel, A.; Stephens, P. J. *Biochemistry* **1994**, *33*, 10911.

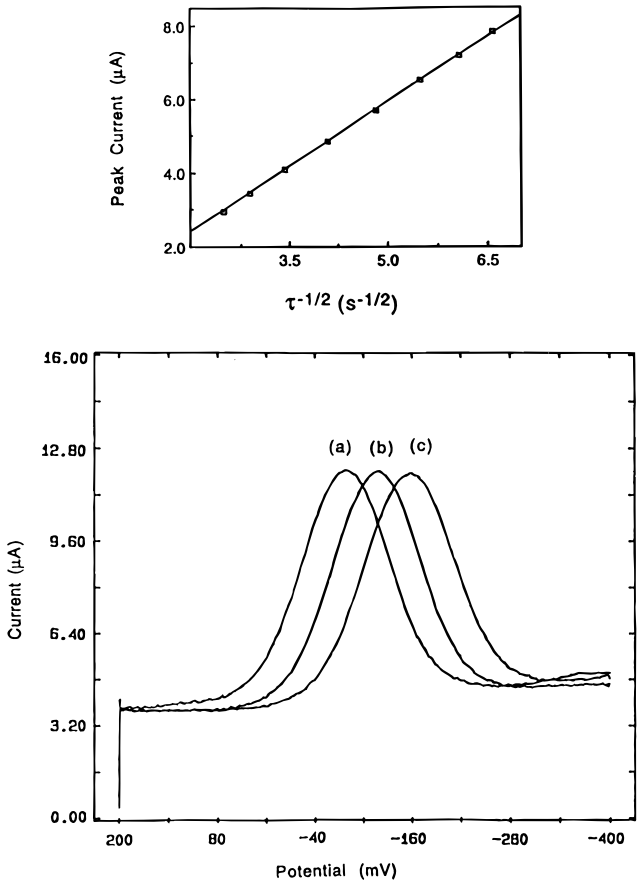


**Figure 8.** Square-wave voltammograms of Rd*Cp* proteins (0.08 mM in 30 mM Tris−HCl (pH, 7.4) and 0.1 M NaCl): (a) recombinant; (b) G10V; (c) G10V/G43V. Conditions: $E_p = 50$ mV, $E_s = 1$ mV, and $\tau^{-1} = 30$ Hz. Inset: plot of the peak current, $I_p$, versus the square root of the frequency of the applied potential pulse, $\tau^{-1/2}$, for the recombinant protein.

mutations upon these factors for the Fe(II) and Fe(III) forms must await further work. One intriguing aspect is that the sum of the potential shifts for the single mutants predicts the experimental shifts of the G10V/G43A and G10V/G43V double mutants (Table 7). Confirmation of such an additivity must await generation of further mutants.

**Conclusions.** Mutation of conserved residues G10 and G43, related by a pseudo-2-fold symmetry, to alanine and valine leads to stable mutant forms of Rd*Cp*. Physical properties are perturbed by the steric interactions between the $\beta$- and $\gamma$-carbon substituents of the new side chains and the CO functions of C9 and C42 and other adjacent groups.

Substitution of Fe(III) by Cd(II) leads to significant structural change at the metal site and in the NH···S distances, in particular (Table 4). Such changes must temper the interesting and significant conclusions made concerning electron transfer mechanisms for native rubredoxins from study of Cd(II)- and Hg(II)-substituted forms.[22] The present mutations produce further perturbation of the chelate loops 5−11 and 38−44 in the Cd(II) derivatives (Figures 3 and 4). $^1$H NMR results (Table 5) indicate that the isopropyl side chain of V10 in the G10V mutant occupies the surface pocket defined by loop 5−11 and thereby modifies the environment of the 5−11 NH protons. The equivalent side chain of V43 in G43V is denied the same access to the 38−44 pocket. This leads to a specific perturbation of the V44−NH···S−C42 interaction in this mutant. These effects are additive in the double mutant G10V/G43V, consistent with the different structural changes being localized in each loop, to a first approximation.

Given the similar surface features of the native Fe(III) and recombinant Cd(II) molecules,[4,39] similar differentiation of properties might be expected in the Fe(III) mutants. This is apparent in the half-wave potentials where, again, an additivity of the differential effects is seen in the double mutants (Table 7). Minor changes in resonance Raman and electronic spectra are dominated by mutation at G10.

Interestingly, similar mutations in the 2[$Fe_4S_4$]-ferredoxin from *Cp* did not affect potentials significantly,[26] nor did mutation of surface carboxylates to carboxamides.[27] Of course, detailed effects will vary from system to system (cf. ref 51). Overall, the present work represents a beginning in the systematic exploration of the influence of the protein chain upon the fundamental properties of this molecule.

**Acknowledgment.** The work was supported by Australian Research Council Grant A29330611 to A.G.W. Sharon McDowell and Prof. Nick Hoogenraad provided valuable support in the initial stages of this work. Mr. Ian Thomas and Dr. John Traeger (La Trobe University) are thanked for skilled technical assistance with mass spectrometry.

IC951653X

(48) Backes, G.; Mino,Y.; Loehr, T. M.; Meyer, T. E.; Cusanovich, M. A.; Sweeney, W. V.; Adman, E. T.; Sanders-Loehr, J. *J. Am. Chem. Soc.* **1991**, *113*, 2055.
(49) Walters, M. A.; Dewan, J. C.; Min, C.; Pinto, S. *Inorg. Chem.* **1991**, *30*, 2656.
(50) (a) Shenoy, V. S.; Ichiye, T. *Proteins: Struct. Funct. Genet.* **1993**, *17*, 152. (b) Yelle, R. B.; Park, N.-S.; Ichiye, T. *Proteins: Struct. Funct. Genet.* **1995**, *22*, 154.
(51) Butt, J. N.; Sucheta, A.; Martin, L. L.; Shen, B.; Burgess, B. K.; Armstrong, F. A. *J. Am. Chem. Soc.* **1993**, *115*, 12587.